Monte Carlo Simulation of a Rarefied Multiphase Plume Flow

Jonathan M. Burt [*] and Iain D. Boyd [†]
Department of Aerospace Engineering
University of Michigan, Ann Arbor, MI 48109

A method for the simulation of flows involving a disperse particle phase and a rarefied gas is extended for increased accuracy and efficiency in modeling the high altitude plume flow from a solid propellant rocket. First, a procedure is presented so that calculations involving the interphase transfer of momentum and energy may be avoided in regions where these calculations will have negligible impact on bulk flow properties. A model for nonequilibrium particle phase change is then described, and a series of simulations is performed for the plume flow from a subscale solid propellant rocket exhausting into a vacuum.

Nomenclature

N_g	=	number of computational gas molecules in a cell
N_p	=	number of computational solid particles in a cell
L	=	global characteristic length scale of the flow
m_j	=	mass of an individual particle
m_g	=	average gas molecule mass
m_p	=	average particle mass
V_{cell}	=	cell volume
n_g	=	gas number density
n_p	=	particle number density
ρ_g	=	gas density
ρ_{mp}	=	particle material density
r_j	=	radius of an individual particle
r_1	=	ratio of crystallization front radius to r_j
D_p	=	average particle diameter
T_j	=	temperature of an individual particle
T_p	=	average particle temperature
T_m	=	equilibrium melting temperature
T_f	=	maximum temperature for homogeneous crystallization
C_{sp}	=	specific heat of particle material
h_f	=	latent heat of fusion
Δt	=	local time step
$\dot{Q}_p$	=	rate of heat transfer to a particle
τ	=	particle thermal accommodation coefficient
k_B	=	Boltzmann's constant
$\mathbf{u}_i$	=	velocity of a computational gas molecule
$\mathbf{u}_j$	=	velocity of an individual particle
$\mathbf{u}_g$	=	local gas bulk velocity
$\mathbf{u}_p$	=	average particle velocity
c_p	=	magnitude of average particle velocity
c_{g1}	=	bulk speed of gas

---

[*] Graduate student, AIAA student member.
[†] Professor, AIAA associate fellow.

American Institute of Aeronautics and Astronautics
Approved for public release; distribution unlimited.

$$c_{g2} = \left(\frac{1}{N_g}\sum_{i=1}^{N_g}\mathbf{u}_i \cdot \mathbf{u}_i\right)^{1/2} \qquad = \text{ rms gas molecule speed}$$

$$c_{r1} = |\mathbf{u}_p - \mathbf{u}_g| \qquad\qquad\quad = \text{ magnitude of difference in average velocities}$$

$$c_{r2} = \frac{1}{N_g}\sum_{i=1}^{N_g}|\mathbf{u}_i - \mathbf{u}_p| \qquad = \text{ average gas molecule speed relative to } \mathbf{u}_p$$

$$c_{r3} = \left(\frac{1}{N_g}\sum_{i=1}^{N_g}|\mathbf{u}_i - \mathbf{u}_p|^2\right)^{1/2} \qquad = \text{ rms gas molecule speed relative to } \mathbf{u}_p$$

f_p =   average interphase collision frequency per particle
C_1 =   cutoff value for gas-to-particle coupling
C_2 =   cutoff value for particle -to-gas coupling

I.   Introduction

EXHAUST flows from solid propellant rockets are characterized by a number of complex and often overlooked phenomena which may significantly affect results in the numerical modeling of these flows. In the propellant grain of a typical solid rocket motor (SRM), a 10 to 20% mass fraction of aluminum powder is used to reduce combustion instabilities and increase specific impulse. Within the combustion chamber, this aluminum content undergoes a complicated process of melting, heterogeneous combustion, evaporation, agglomeration, and breakup. Liquid alumina (Al_2O_3) droplets are expelled through the nozzle entrance, with a bimodal droplet size distribution comprising 100 μm scale agglomerate particles and much smaller smoke particles.[1]

As the gas rapidly expands and cools within the nozzle, significant particle velocity and temperature lags develop, both of which are highly dependent on particle size. Combustion, condensation, agglomeration and breakup processes may continue through the nozzle, and particle phase change becomes important in both the nozzle and nearfield plume regions. Crystallization fronts form and progress within supercooled liquid droplets, heating the particles as they form metastable then stable polycrystalline structures. For the largest particles, this phase transition may continue far into the plume. As a result of these processes, complicated distributions of particle size, temperature, number density, velocity and phase composition often exist in the plume, with a strong dependence on propellant type, nozzle geometry, combustion chamber pressure, and several other factors.[2] In the performance, contamination or radiation analysis of SRM plume flows, various properties of these alumina particles must be considered, and accurate modeling capabilities are desired for the dominant physical phenomena.

Many of the processes involved have been subject to extensive experimental study, and several computational fluid dynamics (CFD) codes currently exist for the analysis of low to medium altitude SRM plume flows.[3] However, little effort has been devoted to the analysis of such plumes at higher altitudes, where traditional CFD methods often break down due to nonequilibrium characteristics within the gas. In order to avoid the loss of accuracy and stability in CFD modeling of such flows, and to better model rarefaction effects in gas-particle momentum and energy exchange, a project is currently underway to develop and implement techniques for plume flow simulation involving the direct simulation Monte Carlo (DSMC) method.[4] This probabilistic method has been shown to overcome deficiencies of CFD in the simulation of rarefied plume flows,[5] and allows a kinetic theory approach to be used in modeling gas-particle interactions.

A DSMC model for the momentum and energy transfer to a spherical solid particle from a surrounding locally free-molecular monatomic gas has been developed by Gallis et al.[6] Following implementation in the DSMC program MONACO[7] and experimental validation, this model has been extended for two-phase flow simulations involving polyatomic gas mixtures, nonspherical particles, and two-way interphase coupling of both momentum and energy.[8,9] A further extension of the model accounts for various effects of solid particle rotation, including force, moment, and heat transfer contributions.[10] The current effort involves the development, implementation and evaluation of additional techniques to increase accuracy and computational efficiency in the simulation of high altitude SRM exhaust plumes.

While the DSMC method allows for a high degree of accuracy in the simulation of rarefied gas flows, excessive computational cost is often cited as a major drawback. The same is true for the two-phase model described here; calculations are generally very expensive, such that any improvement in efficiency will help extend the applicability of the method to larger-scale flows. With this in mind, a series of coupling parameters are developed to

American Institute of Aeronautics and Astronautics

quantitatively evaluate the importance of interphase momentum and energy exchange for both the particles and gas. If coupling in a particular direction and location is determined to have a negligible effect on bulk flow characteristics, corresponding calculations for momentum or energy exchange can then be avoided, and the overall numerical efficiency will increase. In the current implementation, four different nondimensional parameters are periodically evaluated in each cell within the DSMC grid, and time-averaged parameter values are compared to set cutoff values to assess the significance of interphase coupling in either direction. Derivations are provided for all parameters, and a time-averaging scheme used to reduce memory requirements is described.

Propulsive efficiency, particle radiation, particle size distributions and other flow characteristics are strongly dependent on the phase composition of particles within the nozzle and plume.[3] At the nozzle exit plane, the smallest particles are typically made up of some combination of stable α and metastable γ solid phases, while the largest particles consist entirely of liquid alumina. Particles of intermediate size may exist as multiphase "slush balls" within the plume nearfield region, where finite-rate crystallization kinetics and steam release allow for combinations of liquid, multiple solid phases, and trapped water vapor within a single particle.[11] Phase composition and phase change processes will have direct and significant effects on the refractive index and the temperature distribution for the particles, as well as other flow characteristics which may be of interest. Accurate plume simulation therefore requires the consideration of particle phase change, particularly the initial crystallization process for liquid alumina.

A nonequilibrium particle phase change model is presented here, following equations of Henderson,[12] Hunter et al.[13] and Plastinin et al.[14] In this model, it is assumed that homogeneous crystallization begins on the surface of a liquid droplet, at a nucleation temperature well below that required for equilibrium melting. A heterogeneous crystallization front then progresses toward the particle center, at a velocity which varies as a function of the particle temperature. During this process, the particle temperature may either increase or decrease, depending on the balance between convective heat transfer and heat release during crystallization. A simple model for particle melting[13] is also implemented, in order to account for any phase change effects associated with particle-shock interactions. Following a detailed description of the phase change model, results from a series of subscale plume flow simulations are used to indicate the potential importance of particle phase change, and to find appropriate cutoff values for the determination of regions with significant interphase coupling.

II. Interphase Coupling Parameters

To reduce the computational cost of two-phase DSMC plume flow simulations, calculations for momentum and energy exchange between the gas and particles should ideally be made only where the flow is locally determined to involve significant one or two-way interphase coupling. A series of coupling parameters are proposed so that this determination may be made automatically during a simulation. Regions of interphase coupling are identified through the periodic evaluation of these coupling parameters in each cell within the computational grid, and a comparison is then made of parameter values with cutoff values set by the user. Four separate coupling parameters are used here: A parameter P_{1m} quantifies the importance of momentum coupling from the gas to the particles; a smaller value of P_{1m} indicates that the gas has less influence on the particle phase momentum flux. A second parameter P_{1e} relates to energy coupling from the gas to the particles, while parameters P_{2m} and P_{2e} indicate the significance of momentum and energy coupling, respectively, from the particles to the gas. These parameters are formulated with the goal of minimizing the cost of parameter evaluations, while allowing for reasonable accuracy over a wide range of flow regimes.

The gas-to-particle momentum coupling parameter P_{1m} is defined here to scale with the fractional change in average particle speed, due to interphase momentum transfer, over a streamwise distance L. The variable L here represents some global characteristic length scale; for a plume flow we set L to equal the nozzle exit diameter. Neglecting spatial variation in the particle speed gradient ∇c_p, it follows that

$$P_{1m} \propto \frac{1}{c_p}\left(L\frac{\mathbf{u}_p}{c_p}\right)\bullet\nabla c_p = \frac{\partial c_p}{\partial t}\frac{L}{c_p{}^2}. \tag{1}$$

To evaluate the $\dfrac{\partial c_p}{\partial t}$ term, we use the fact that $m_p\dfrac{\partial c_p}{\partial t}$ is roughly equal to the product of the average interphase collision frequency f_p for a single particle and the magnitude of the average momentum transferred per collision. (In the special case where every particle in the cell has the same mass and velocity, it can be shown that $m_p\dfrac{\partial c_p}{\partial t}$ is equal

American Institute of Aeronautics and Astronautics

to the dot product of this average momentum transfer and $f_p \mathbf{u}_p/c_p$.) If all particles are much larger than gas molecules, then the collision frequency will be roughly $\frac{1}{4}\, \pi n_g c_{r2} D_p^2$ assuming that the thermal speed of the particle phase is small.

In determining the average momentum transfer per collision, we assume that all particles are much more massive than gas molecules, and that following an interphase collision the gas molecule velocity is on average equal to that of the particle. As shown in a recent paper,[9] the latter assumption is exact for specularly reflecting collisions involving spherical particles or convex particles of arbitrary orientation, and is a reasonably good approximation for diffusely reflecting collisions. Under these assumptions, the average momentum transfer magnitude is roughly equal to $m_g c_{r1}$, so the magnitude of the average force exerted by the gas on a single particle can be given as

$$m_p \frac{\partial c_p}{\partial t} = f_p\, m_g c_{r1} = \frac{1}{4}\, \pi \rho_g\, c_{r2}\, D_p^2\, c_{r1} \ . \tag{2}$$

Next, Eq. (2) is rearranged and substituted into Eq. (1), and the average particle mass m_p is approximated as $\frac{\pi}{6}\rho_{mp}D_p^3$. Ignoring a multiplicative constant of order one, we then have the final formulation for the momentum coupling parameter P_{1m}:

$$P_{1m} = \frac{\rho_g}{\rho_{mp}} \frac{c_{r1}c_{r2}}{c_p^2} \frac{L}{D_p} \tag{3}$$

The parameter P_{2m} which characterizes momentum coupling from the particles to the gas is derived in a similar manner. Following Crowe et al.,[15] P_{2m} is proportional to the magnitude of the total drag force on the particle phase per unit volume, divided by the streamwise gas momentum flux and nondimensionalized through multiplication by the length scale L. The streamwise gas momentum flux is approximated here as $\rho_g c_{g1}^2$, and from Eq. (2) the magnitude of the force per unit volume is $\frac{1}{4}\, \pi\rho_g\, c_{r2}\, D_p^2\, c_{r1}\, n_p$. Neglecting a constant of order one, the parameter P_{2m} may then be defined by

$$P_{2m} = n_p D_p^2 L \frac{c_{r1}c_{r2}}{c_{g1}^2} \ . \tag{4}$$

In comparing Eqs. (3) and (4), note that an identical formulation for P_{1m} could be found by substituting an approximate particle momentum flux $m_p n_p c_p^2$ for the gas momentum flux in the derivation of P_{2m}. The above derivation for Eq. (3) is used only to show the physical significance of this parameter.

The definition of the parameter P_{1e} for energy coupling from the gas to the particles is analogous to that of P_{1m}: Here P_{1e} scales with the fractional change in average particle temperature over a streamwise distance L.

$$P_{1e} \propto \frac{1}{T_p}\left(L\frac{\mathbf{u}_p}{c_p}\right)\bullet \nabla T_p = \frac{\partial T_p}{\partial t} \frac{L}{c_p T_p} \tag{5}$$

The time-derivative of T_p is related to the average heat transfer rate $\dot{Q}_p$ per particle by $\dot{Q}_p = C_{sp} m_p \frac{\partial T_p}{\partial t}$. Approximating m_p as $\frac{\pi}{6}\rho_{mp}D_p^3$, we then have

$$P_{1e} \propto \left(\frac{6}{\pi}\frac{\dot{Q}_p}{\rho_{mp}D_p^3 C_{sp}}\right)\frac{L}{c_p T_p} \ . \tag{6}$$

Note that $\dot{Q}_p$ is equal to the product of the interphase collision frequency f_p and the average heat transfer per collision. To evaluate the latter term, a few initial assumptions are used: First, we assume that the interphase heat transfer process is dominated by the exchange of gas translational energy. It is also assumed that the ratio of $|\mathbf{u}_p - \mathbf{u}_g|$

American Institute of Aeronautics and Astronautics

to the local sonic speed of the gas (the average particle Mach number) is much less than one. Under such conditions the mean translational energy of a colliding gas molecule in a particle-centered coordinate system can be approximated as $\frac{2}{3} m_g c_{r3}^2$. If the collision involves diffuse reflection with full thermal accommodation to the particle temperature, then the average post-collision translational energy will be $2k_B T_p$. Otherwise specular reflection is assumed, and the gas molecule will retain its initial translational energy relative to the particle. From the above approximations, it follows that

$$\dot{Q}_p = \frac{\pi}{6} n_g c_{r2} D_p^{\ 2} \tau \left(m_g c_{r3}^2 - 3 k_B T_p \right). \tag{7}$$

By definition, all coupling parameters here must be greater than or equal to zero, so the absolute value of $\dot{Q}_p$ is used in the equation for P_{1e}. Substitution into Eq. (6) then gives the following result:

$$P_{1e} = \frac{L}{D_p} \frac{c_{r2}}{c_p} \frac{\rho_g}{\rho_{mp}} \frac{\tau}{C_{sp} T_p} \left| c_{r3}^2 - \frac{3k_B T_p}{m_g} \right| \tag{8}$$

While Eq. (8) has been derived for a flow in which the average particle Mach number is low and gas internal energy transfer is negligible during interphase collisions, this parameter should be able to accurately characterize energy coupling over a very wide range of flow regimes. If, for example, the parameter were derived under the assumption that the particles move hypersonically with respect to the gas, the coefficient 3 in Eq. (8) would be replaced by 4, and all other terms would be identical. Moreover, this last term becomes negligible in comparison with c_{r3}^2 as the relative Mach number increases, so that Eq. (8) should be equally valid at the high and low Mach number limits.

The final coupling parameter P_{2e}, which determines the importance of energy coupling from the particle phase to the gas, has a similar definition to that of P_{2m}. Again following Crowe et al.,[15] P_{2e} is proportional to the interphase energy transfer rate $\dot{E}$ per unit volume, and inversely proportional to the streamwise energy flux of the gas Φ_g. In determining the energy transfer rate, we neglect particle rotation effects and assume that all particles are much more massive than gas molecules. It follows from these assumptions that $\dot{E} = \dot{Q}_p n_p$, so nondimensionalization by the length scale L gives the relation $P_{2e} \propto \dot{Q}_p n_p L / \Phi_g$. Here $\dot{Q}_p$ is given by Eq. (7), and the energy flux Φ_g is approximated as the product of the streamwise gas number flux and the average energy per molecule. For simplicity we consider the special case of a monatomic simple gas, where the latter term will equal $\frac{1}{2} m_g c_{g2}^2$ and $\Phi_g \approx \frac{1}{2}\rho_g c_{g1} c_{g2}^2$. Neglecting a coefficient of order one, substitution into the above relation for P_{2e} gives the formula

$$P_{2e} = n_p L D_p^{\ 2} \frac{c_{r2}}{c_{g1} c_{g2}^2} \tau \left| c_{r3}^2 - \frac{3k_B T_p}{m_g} \right|. \tag{9}$$

As implemented in the DSMC code MONACO[7] for two-phase flow simulations, all four coupling parameters are periodically evaluated at each cell within the computational grid. For the local determination of interphase coupling, a few additional symbols are required: Let C_1 represent a user-defined cutoff value for momentum or energy coupling from the gas to the particle phase, and define C_2 as the equivalent value for coupling from the particles to the gas. If $\max\{P_{1m}, P_{1e}\} \geq C_1$ then a parameter Ψ_1 is set to equal one; otherwise Ψ_1 will equal zero. A similar parameter Ψ_2 will be one if $\max\{P_{2m}, P_{2e}\} \geq C_2$ or zero if $\max\{P_{2m}, P_{2e}\} < C_2$. Next, define $\langle\Psi_1\rangle$ and $\langle\Psi_2\rangle$ as the average of a large number of evaluations of Ψ_1 and Ψ_2, respectively, in a given cell. In the case of a steady flow simulation, these averages are taken over all values since steady state is first attained.

The values of $\langle\Psi_1\rangle$ and $\langle\Psi_2\rangle$ are then used to determine the importance of coupling. At any given cell, interphase momentum and energy transfer are assumed to significantly affect particle properties only if $\langle\Psi_1\rangle \geq \frac{1}{2}$. (This is equivalent to the condition that $\max\{P_{1m}, P_{1e}\} \geq C_1$ is satisfied at least 50% of the time.) Various properties of

particles in the cell are therefore altered due to particle-gas interaction only if this condition is met. Otherwise all related calculations are avoided, and numerical efficiency is improved through a reduction in the total number of operations. Similarly, calculations used in modifying local gas phase properties are only performed if $\langle\Psi_2\rangle \geq \frac{1}{2}$. This procedure should greatly reduce the overall computational cost of a variety of two-phase DSMC simulations, particularly those for the high altitude SRM plume flows of interest, where interphase coupling in either direction may be significant only within a small fraction of the flowfield under consideration.

III.   Particle Phase Change

As discussed above, the phase composition of an individual particle within an SRM plume flow is typically a strong function of particle size, position in the plume, nozzle geometry and several other factors. Phase change processes will in turn influence the particle temperature, as well as that of the surrounding gas, and may greatly affect radiative properties throughout the plume. Several previous studies involving SRM exhaust flow simulations have included consideration of the nonequilibrium phase change processes typical to such flows,[3,12] but little effort has been devoted to the detailed characterization of particle phase composition in high altitude plume flows, where gas-particle interactions must be considered through a kinetic theory based approach.

Following the model of Hunter et al.,[13] we consider only the dominant crystallization process involving formation of the metastable γ phase, and neglect the γ-to-α transition which typically occurs among smaller particles in the nearfield plume region. However, this omission is corrected in part by the fact that the value used here for the latent heat of fusion ($h_f = 1.07\times10^6$ J/kg) accounts for the full transition of particle material from liquid alumina to the stable α phase. The standard model for crystallization kinetics in alumina particles involves an assumption that the phase change process is initiated only after a spherical liquid droplet has supercooled to a nucleation temperature T_f significantly below the equilibrium melting temperature T_m. Once this occurs, nucleation takes place uniformly over the outer surface of the particle, and a heterogeneous crystallization front then progresses toward the particle center at a rate given by

$$\frac{dr_l}{dt} = -\frac{A}{r_j}(T_m - T_j)^n \tag{10}$$

where T_j and r_j are the particle temperature and radius respectively, r_l is the ratio of the crystallization front radius to r_j, and A and n are constants with $A = 2.7\times10^{-6}$ ms^{-1}K$^{-1.8}$ and $n = 1.8$ as given by Plastinin et al.[16] This variation in r_l in turn affects the particle temperature through the energy balance equation

$$C_{sp}\, m_j\, \frac{dT_j}{dt} = \dot{Q}_j - 3\, h_f\, m_j\, r_l^2\, \frac{dr_l}{dt}\;. \tag{11}$$

As currently implemented, the relation between the interphase heat transfer rate $\dot{Q}_p$ and the temporal variation in particle temperature is divided into three separate cases: solidification, melting, and constant-phase heating or cooling. First, if $T_j < T_f$ and $r_l = 1$, or if $T_j < T_m$ and $r_l \in (0,1)$, then the particle is determined to be in the process of solidification, and r_l is updated according to Eq. (10). The temperature change ΔT_j is then given by

$$\Delta T_j = \frac{\dot{Q}_j\, \Delta t}{C_{sp}\, m_j} - \frac{h_f}{C_{sp}}\Delta\left(r_l^3\right) \tag{12}$$

where $\Delta(r_l^3)$ is the variation in r_l^3 during the time step of length Δt. This case must be considered for all particles throughout the grid domain, even in regions where gas-to-particle coupling is neglected. The relatively large local Δt values which can be encountered for solidifying particles within uncoupled regions may produce large discretization errors in ΔT_j, such that T_j can exceed the melting temperature T_m. To avoid this possibility, a variable N is set to equal the smallest integer for which $N > 50\times\Delta T_j/T_m$. If $N > 1$ then the initial values of T_j and r_l are reassigned to the particle, the time step is divided into N intervals of length $\Delta t/N$, and the above procedure is iteratively repeated N times to find the final values of T_j and r_l.

American Institute of Aeronautics and Astronautics
Approved for public release; distribution unlimited.

If $T_j \geq T_m$, $r_1 < 1$ and $\dot{Q}_p > 0$, then the particle is in the process of melting. In this case we assume that T_j is held constant and all thermal energy transferred to the particle is used in the phase transition. Note that for a melting particle, the normalized crystallization front radius r_1 does not physically represent a phase transition surface, but is used instead to record the cube-root of the liquid volume fraction. The current implementation enforces energy conservation by allowing for the special case when, in a single time step, the last solid material in the particle melts and the remaining collision energy is used to increase the particle temperature. Following Hunter et al.,[13] the normalized front radius is first updated according to Eq. (12), where ΔT_j is set equal to zero. If the resulting r_1 value is greater than one, then the particle temperature is increased by

$$\Delta T_j = \frac{h_f}{C_{sp}} \left(r_1^3 - 1 \right) \tag{13}$$

after which r_1 is set to equal one. In the last case, where the particle is neither solidifying nor melting, the temperature is varied as

$$\Delta T_j = \frac{\dot{Q}_j \Delta t}{C_{sp} m_j} \tag{14}$$

following the standard procedure for Lagrangian tracking of single-phase particles.

IV.   Plume Flow Test Case

In order to evaluate the above models, demonstrate capabilities of the code, and determine appropriate coupling parameter cutoff values, simulations are performed for a subscale SRM plume exhausting into a vacuum. Inflow conditions along the nozzle exit plane are based on values provided by Anfimov et al.[17] for a Star 27 SRM used in the Bow Shock Ultraviolet 2 test flight, with dimensions reduced by a factor of 10 for a nozzle exit inner diameter of 7.8 cm. While the reduction in scale should ideally be accompanied by increases in particle velocity and temperature lags, the goal here is to simulate a representative plume flow, so this error source can be tolerated with the understanding that the precise modeling of an actual flow is not desired here. The scale reduction allows for a dramatic decrease, by about two orders of magnitude, in overall computational cost.

The gas here consists of a mixture of H_2, CO and N_2, and particles are divided into a discrete size distribution with seven diameter values ranging from 0.3 to 6 μm. The mass flow rate through the nozzle for each particle size is shown in Fig. 1. Initial particle phase compositions are based on equilibrium phase change calculations, such that the largest particles are entirely liquid and the smallest particles have a liquid mass fraction of 58% at the nozzle exit. An axisymmetric simulation is performed, with an unstructured rectangular grid extending from the nozzle exit 100 m downstream and 40 m outward from the central axis. The simulation is repeated for several different coupling parameter cutoff values, where values for both gas-to-particle and particle-to-gas coupling are equal and range from 0 to 0.1. Each case requires about 200 cpu hours on four 1.4 GHz AMD Opteron processors. Selected simulation results are shown in Figs. (2) through (12).

Figure (2) shows the variation in the maximum downstream distance for interphase coupling in either direction as a function of the cutoff values. Except for the largest cutoff values considered, the length of the coupling domain is found to vary as roughly the inverse square-root of the corresponding cutoff value, so that a smaller cutoff value results in a greater residence time for either particles or gas molecules within the flowfield region where they may be influenced by interphase momentum or energy transfer. In Fig. (3), the axial component of velocity for the smallest particle size is plotted as a function of the cutoff value for gas-to-particle coupling, at two different points located 50 m downstream from the nozzle exit plane and distances of 3.5 m and 14 m from the central axis. Corresponding plots are given as Figs. (4) and (5) for particles of intermediate size (1 μm diameter) and for the largest particles, respectively. As shown on all three plots, farfield particle velocity varies significantly with the cutoff value C_1 for $C_1 > 10^{-4}$, while a relatively weak dependence is found for $C_1 \leq 10^{-4}$.

A similar trend is found in Figs. (6) through (8), which show the variation with C_1 in particle temperature at the same two locations. Again particle temperature is generally found to be a strong function of the cutoff value only for $C_1 > 10^{-4}$. The one exception to this trend is found in Fig. (7), for 1 μm diameter particles at the point (50, 3.5). In this case, the average particle temperature initially decreases as C_1 is reduced from the maximum value of 0.1, due to the corresponding increase in particle residence time within the gas-to-particle coupling region where heat is

American Institute of Aeronautics and Astronautics
Approved for public release; distribution unlimited.

transferred from particles to the colder surrounding gas. However, for $C_1 < 10^{-3}$ the average particle temperature increases as C_1 is further reduced. This is explained by the fact that for this particular case, the residence time of 1 μm particles within the gas-to-particle coupling region is great enough for a fraction of the initially liquid particles to cool below the homogeneous crystallization temperature T_f = 1930 K. Once the temperature of a liquid particle reaches T_f, the solidification process immediately begins and the particle temperature increases following the energy balance of Eq. (11). The fraction of 1 μm particles for which this process takes place will increase for smaller values of C_1, so the average temperature of these particles will increase.

This trend is further illustrated by Fig. (9), which shows the variation in liquid mass fraction with C_1 for the same particle size and location. For $C_1 > 10^{-3}$ all 1 μm particles at this point are found to be entirely liquid, while the liquid mass fraction decreases for smaller C_1 to a value of 0.728 at C_1 = 0. In both Figs. (7) and (9) the data point for C_1 = 0 is represented by a horizontal line through the vertical axis. Note that all other data sets in Figs. (6) to (8) show monotonic trends through the full C_1 range, as the phase composition for these cases does not vary as a function of C_1. At both locations and for all C_1 values considered here, all 0.3 μm particles have completely solidified, and all 6 μm particles are entirely liquid. In addition, 1 μm particles are entirely liquid at the point (50,14) due to the reduced interphase heat transfer which results from the relatively low gas number density far from the axis.

Various gas properties were examined at the same two flowfield locations, to determine any dependence on the cutoff value C_2 for particle-to-gas coupling. Of the properties considered, only a weak dependence could be found for the gas translational temperature, while the variation in all other properties was within statistical scatter. The lack of C_2 dependence can be attributed to the very small domains for particle-to-gas coupling, as well as the dominance of the expansion process over interaction with the particle phase in determining bulk gas properties far from the nozzle.

Figure (10) shows the variation with cutoff values ($C_1 = C_2$) in overall simulation efficiency. The vertical axis here gives the total cpu time per time step at steady state, normalized by the corresponding value when both cutoff values are set to zero. As expected, simulation time is shown to decrease monotonically as cutoff values are increased. For a given level of precision in simulation results, the use of coupling parameters allows for a roughly 20% reduction in calculation time when cutoff values are set to 10^{-6}, or a 65% reduction when these values are set to 0.1. A cutoff value of 10^{-4} is therefore recommended for both C_1 and C_2, to balance overall numerical efficiency and accuracy in results for both the particles and gas. As shown in Fig. (10), the utilization of coupling parameters to identifying regions of negligible interphase coupling results in a 30% reduction in simulation time when this cutoff value is used. While no universal cutoff value can be found to optimize this balance under all flow conditions, particularly when particle phase change is important, a value of 10^{-4} can in general be expected to provide both reasonably good accuracy and efficiency.

Selected results for the case where $C_1 = C_2 = 10^{-4}$ are displayed in Figs. (11) and (12). Figure (11) shows the contours of mass-averaged particle temperature (top) and gas translational temperature. As expected, particle temperatures are uniformly higher than that of the surrounding gas, with the lowest particle temperatures occurring far from the central axis where the smaller particles are concentrated. A slight reduction in average particle temperature is found close to the axis, as a result of the increased heat transfer toward the center of the plume nearfield region where the gas number density is greatest. Contours of the Sauter mean particle diameter are shown in Fig. (12), along with the overall liquid mass fraction for the particles. (The Sauter mean diameter is the diameter of a particle with a volume-to-surface area ratio equal to that of the particle phase as a whole.) The concentration of larger particles toward the axis results in a greater content of liquid alumina within this region, as the reduced surface area-to-mass ratio among larger particles allows for a more gradual process of cooling and solidification.

V.   Conclusions and Future Work

A series of parameters has been presented for the evaluation of interphase momentum and energy transfer contributions in a two-phase DSMC simulation. A method was proposed for the use of these parameters in the automatic determination of coupling regions for each phase, involving only two time-averaged variables with values that must be stored for each cell. Through the evaluation of results from a subscale plume test case, we determined a recommended value of 10^{-4} for the two coupling parameter cutoff values used in this method. The implementation of a model for nonequilibrium phase change between liquid and solid states was discussed, and it was shown that the method for determining regions of interphase coupling may unavoidably reduce simulation accuracy in special cases involving particle phase change. For the representative plume flow considered, the recommended coupling parameter cutoff value corresponds to a roughly 30% reduction in total simulation time. While a 30% savings may not be considered sufficiently large to warrant implementation of the method described here, the efficiency increase

American Institute of Aeronautics and Astronautics

may be much greater when the grid is extended to include the full domain of interest for plume radiation signature analysis.

Several complex phenomena may affect bulk flow characteristics in the high altitude SRM plume flows of interest, and additional physical models are currently under development to increase accuracy and output capabilities in the simulation of these flows. An upcoming paper[18] will focus on a Monte Carlo ray trace model for particle radiation, which accounts for radiative heat transfer between non-gray particles in plume flows of arbitrary optical thickness, allows for direct measurements of spectral radiance, and includes consideration of multiple scattering and emission from nozzle walls. Models for particle surface chemistry, including effects of heterogeneous combustion, evaporation and sublimation, will also be implemented in the coming months. Detailed validation will be performed, to the extent possible, through comparison of numerical and experimental results for radiative properties in a full scale plume flow.

Acknowledgments

References

[1]Simmons, F. S., *Rocket Exhaust Plume Phenomenology*, Aerospace Press, El Segundo, CA, 2000, pp. 173-200.

[2]Geisler, R. L., "A Global View of the Use of Aluminum Fuel in Solid Rocket Motors," AIAA Paper 2002-3748, *38th AIAA/ASME/SAE/ASEE Joint Propulsion Conference*, Indianapolis, IN, 2002.

[3]Reed, R. A., and Calia, V. S., "Review of Aluminum Oxide Rocket Exhaust Particles," AIAA Paper 93-2819, 1993.

[4]Bird, G. A., *Molecular Gas Dynamics and the Direct Simulation of Gas Flows*, Clarendon Press, Oxford, 1994, pp. 203-204.

[5]Boyd, I. D., Penko, P. F., Meissner, D. L., and DeWitt, K. J., "Experimental and Numerical Investigations of Low-Density Nozzle and Plume Flows of Nitrogen," *AIAA Journal*, Vol. 30, No. 10, 1992, pp. 2453-2461.

[6]Gallis, M. A., Torczynski, J. R., and Rader, D. J., "An approach for Simulating the Transport of Spherical Particles in a Rarefied Gas Flow via the Direct Simulation Monte Carlo Method," *Physics of Fluids*, Vol. 13, No. 11, 2001, pp. 3482-3492.

[7]Dietrich, S., and Boyd, I. D., "Scalar and Parallel Optimized Implementation of the Direct Simulation Monte Carlo Method," *Journal of Computational Physics*, Vol. 126, 1996, pp. 328-342.

[8]Burt, J. M., and Boyd, I. D., "Evaluation of a Monte Carlo Model for Two Phase Rarefied Flows," AIAA Paper 2003-3496, *36th AIAA Thermophysics Conference*, Orlando, FL, 2003.

[9]Burt, J. M., and Boyd, I. D., "Development of a Two-Way Coupled Model for Two Phase Rarefied Flows," AIAA paper 2004-1351, *42nd AIAA Aerospace Sciences Meeting*, Reno, NV, 2004.

[10]Burt, J. M., and Boyd, I. D., "Particle Rotation Effects in Rarefied Two-Phase Plume Flows," *24th International Symposium on Rarefied Gas Dynamics*, Monopoli, Italy, Monopoli, Italy, 2004.

[11]Gosse, S., Sarou-Kanian, V., Veron, E., Millot, F., Rifflet, J. C., and Simon, P., "Characterization and Morphology of Alumina Particles in Solid Propellant Subscale Rocket Motor Plumes," AIAA Paper 2003-3649, *36th AIAA Thermophysics Conference*, Orlando, FL, 2003.

[12]Henderson, C. B., "Effect of Crystallization Kinetics on Rocket Performance," *AIAA Journal*, Vol. 15, No. 4, 1977, pp. 600-602.

[13]Hunter, S. C., Cherry, S. S., Kliegel, J. R., and Waldman, C. H., "Gas-Particle Nozzle Flows with Reaction and Particle Size Change," AIAA Paper 81-0037, *19th AIAA Aerospace Sciences Meeting*, St. Louis, MO, 1981.

[14]Plastinin, Y. A., Anfimov, N. A., Baula, G. G., Karabadzhak, G. F., Khmelinin, B. A., Rodionov, A. V., "Modeling of Aluminum Oxide Particle Radiation in a Solid Propellant Motor Exhaust," AIAA Paper 96-1879, *31st AIAA Thermophysics Conference*, New Orleans, LA, 1996.

[15]Crowe, C., Sommerfeld, M., and Tsuji, Y., *Multiphase Flows with Droplets and Particles*, CRC Press, New York, 1998, pp. 31-34.

[16]Plastinin, Y. A., Sipatchev, H. P., Karabadzhak, G. F., Khmelinin, B. A., Szhenov, E. Y., Khlebnikov, A. G., Shishkin, Y. N., "Experimental Investigation of Alumina Particles' Phase Transition and Radiation," AIAA Paper 98-0862, *36th AIAA Aerospace Sciences Meeting*, Reno, NV, 1998.

[17]Anfimov, N. A., Karabadjak, G. F., Khmelinin, B. A., Plastinin, Y. A., and Rodinov, A. V., "Analysis of Mechanisms and Nature of Radiation from Aluminum Oxide in Different Phase States in Solid Rocket Exhaust Plumes," AIAA Paper 93-2818, *28th AIAA Thermophysics Conference*, Orlando, FL, 1993.

[18]Burt, J. M., and Boyd, I. D., "A Monte Carlo Radiation Model for Simulating Rarefied Multiphase Plume Flows," *38th AIAA Thermophysics Conference*, Toronto, Canada, 2005 (to be presented).
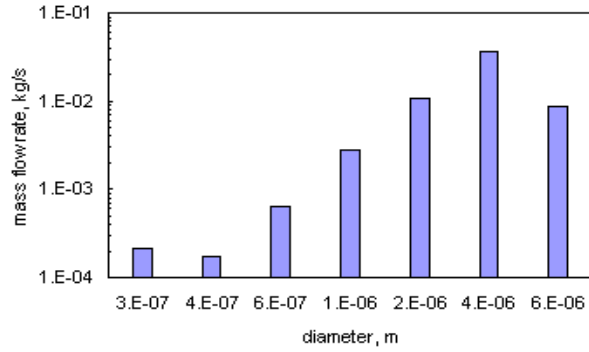
American Institute of Aeronautics and Astronautics

Figure 1. Mass flow rate at nozzle exit for each particle size.
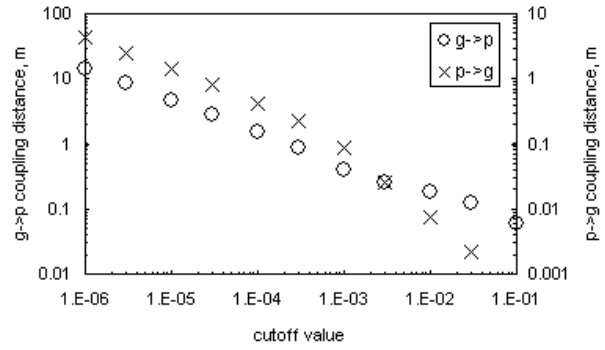

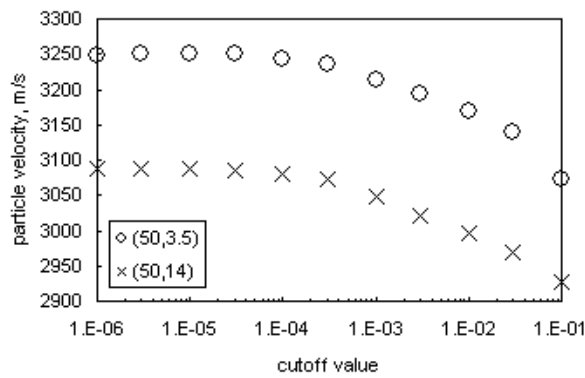**Figure 2. Maximum downstream distance for interphase coupling.**

Figure 3. Axial velocity component for 0.3 μm diameter particles as a function of cutoff value C_1 for gas-to-particle coupling.
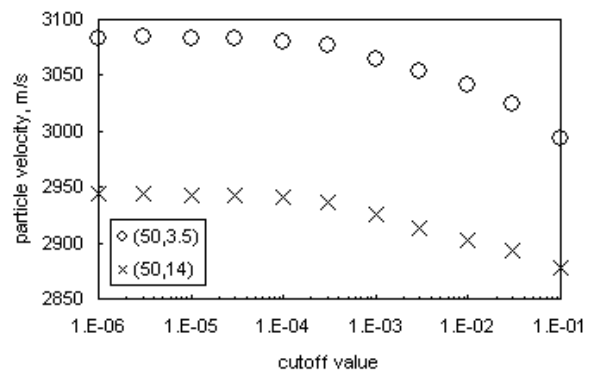

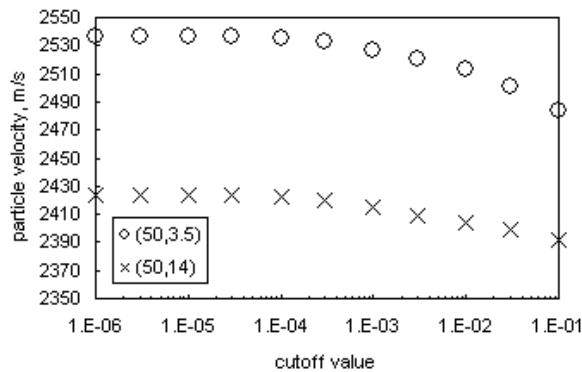**Figure 4. Axial velocity component for 1 μm particles as a function of cutoff value.**

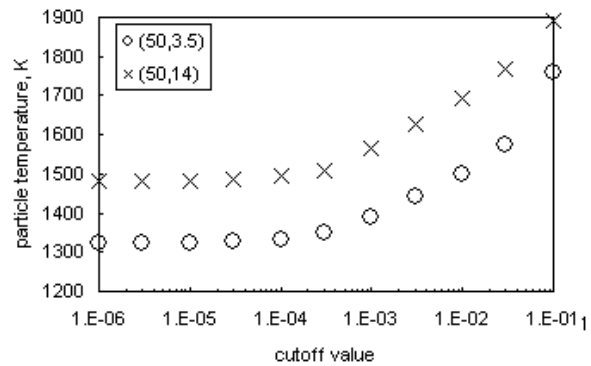**Figure 5. Axial velocity component for 6 μm particles as a function of cutoff value.**

Figure 6. Temperature of 0.3 μm particles as a function of cutoff value.
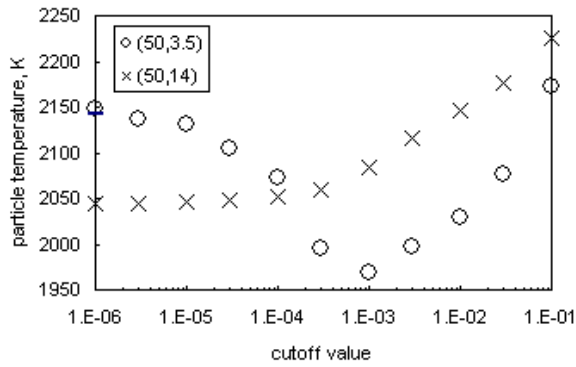
Figure 7. Temperature of 1 μm particles as a function of cutoff value.
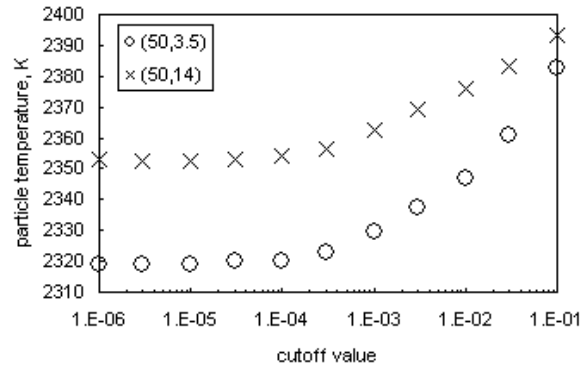
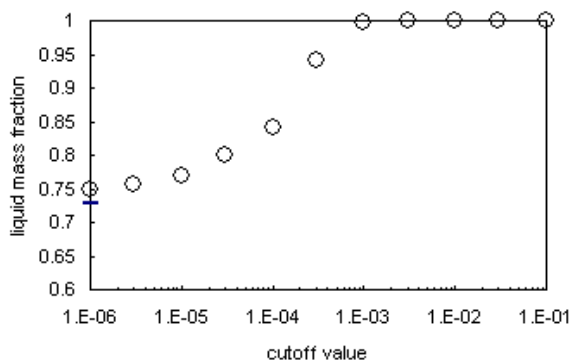**Figure 8. Temperature of 6 μm particles as a function of cutoff value.**

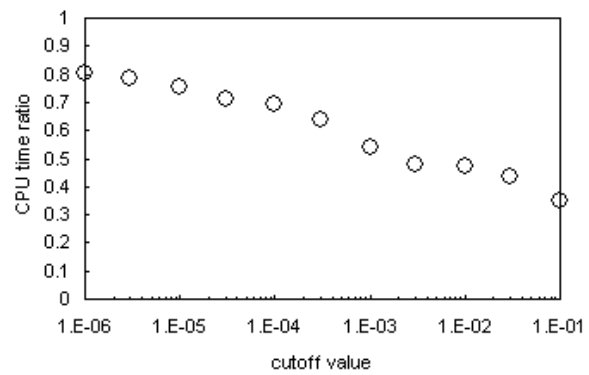**Figure 9. Variation in liquid mass fraction for 1 μm particles at the point (50, 3.5).**

Figure 10. Total cpu time per time step at steady state, normalized by cpu time for the zero cutoff values case.
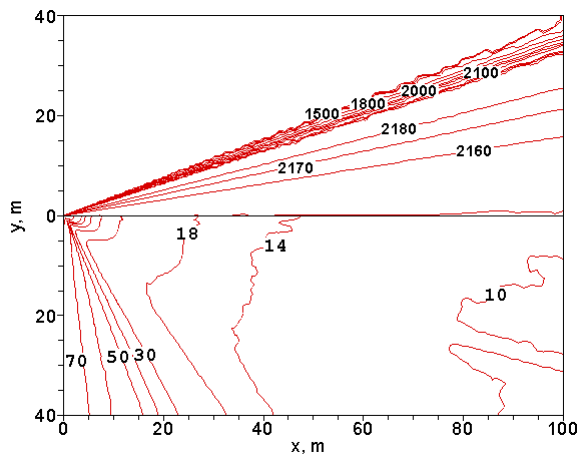

Figure 11. Contours of mass-averaged particle temperature (top) and gas translational temperature. All values are in SI units.
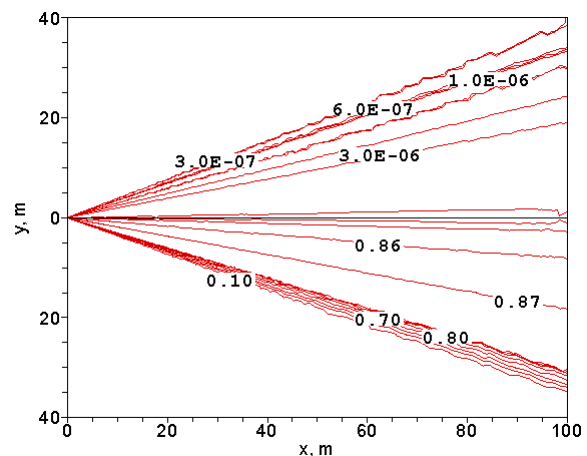

Figure 12. Sauter mean particle diameter (top) and liquid mass fraction of particles.

American Institute of Aeronautics and Astronautics